青年园地

Low-Temperature Oxidation Behavior of $(Zr_{1/3}Nb_{1/3}Ti_{1/3})C$ Solid-Solution Ceramics in Air

YE Beilin, WEN Tongqi, CHU Yanhui
(School of Materials Science and Engineering, South China University of Technology, Guangzhou 510641, China)

Abstract: In order to investigate the low-temperature oxidation behavior of the ternary carbide solid-solution ceramics, the low-temperature oxidation behavior of $(Zr_{1/3}Nb_{1/3}Ti_{1/3})C$ (ZNTC) solid-solution ceramics was investigated by the isothermal-exposure oxidation test at 1073~1473 K in air for 120 minutes. The results showed that ZNTC samples possessed good low-temperature oxidation resistance and their oxidation process could be described by a parabolic rate law. As oxidation temperature increasing from 1073 to 1473 K, the calculated parabolic rate of ZNTC decreased slowly from 1073 to 1173 K, then increased rapidly from 1173 to 1273 K, and finally decreased gradually from 1273 to 1473 K. This behavior was primarily attributed to the evolution of the composition and microstructure in the oxide layers. Specifically, the oxidation products were mainly composed of ZrO_2, Nb_2O_5, and TiO_2 at 1073~1173 K, and then transformed into the composition of $ZrTiO_4$, $TiNb_2O_7$, and $Nb_2Zr_6O_{17}$ at 1273~1473 K. In addition, in the view of surface and cross-section, the morphology feature of oxidation products changed with the oxidation temperature.

Key words: ultra-high temperature ceramics; solid solutions; carbides; microstructure; oxidation
CLC number: TQ174.75 **Document code**: A **Article ID**: 1674-3962(2020)12-0918-06

$(Zr_{1/3}Nb_{1/3}Ti_{1/3})C$ 固溶体陶瓷的低温氧化行为研究

叶贝琳，文通其，褚衍辉
（华南理工大学材料科学与工程学院，广东 广州 510641）

摘 要：为了研究三元碳化物固溶体材料的低温氧化行为，利用等温暴露氧化实验方法研究了$(Zr_{1/3}Nb_{1/3}Ti_{1/3})C$ 固溶体陶瓷在不同低温空气中的氧化行为。研究结果表明，在 1073~1473 K 温度范围内，$(Zr_{1/3}Nb_{1/3}Ti_{1/3})C$ 固溶体陶瓷具有优良的低温抗氧化性能，其氧化动力学符合抛物线规律，氧化过程受氧气在氧化层中的扩散速率控制；随着氧化温度升高，该材料的氧化速率常数表现出先缓慢降低、再迅速增加、最后逐渐降低的趋势。上述结果可主要归因于该陶瓷在不同温度下形成的氧化层的物相组成及微观结构的演变，即该材料在 1073~1173 K 温度下的氧化产物主要是由简单的 ZrO_2、Nb_2O_5 和 TiO_2 相组成，而在 1273~1473 K 温度下的氧化产物主要是由复杂的 $ZrTiO_4$、$TiNb_2O_7$ 和 $Nb_2Zr_6O_{17}$ 相组成，且随着氧化温度的升高，氧化产物的表面微观结构经历了致密-多孔-致密的演变过程，截面微观结构经历了致密-分层-致密的演变过程。

关键词：超高温陶瓷；固溶体；碳化物；微观结构；氧化

1 Introduction

As a class of ultra-high temperature ceramics, transition-metal carbides (TMC) have attracted considerable attentions in recent years owning to their ultra-high melting temperature (up to 4000 K), high hardness, chemical inertness, electrical and thermal conductivity, and low neutron absorption[1, 2]. These distinguished performances are suitable for potential applications in aircraft, atomic and astronautic manufacturing industries[3, 4]. However, widespread application of TMC has been restricted by a limited range of their inherent properties[5-7]. Attempts have been made to develop advanced TMC ceramics with a wider range of properties through the fabrication of multi-component TMC solid-solution ceramics. In the past few years, the diverse TMC solid-solution ceramics with binary[8, 9], ternary[10-12] or more components[13-17], had been successfully fabricated, their thermal-physical, mechanical,

Received date: 2020-04-28 **Revised date**: 2020-07-08
Foundation item: National Natural Science Foundation of China (51802100, 51972116)
First author: YE Beilin, Female, Born in 1994, Master
Corresponding author: CHU Yanhui, Male, Born in 1987, Professor, Email: chuyh@scut.edu.cn
DOI: 10.7502/j.issn.1674-3962.202004021

and electrical properties were also investigated. Recently, the oxidation behavior of a class of binary TMC solid-solution ceramics, namely $Hf_xTa_{1-x}C$, under extreme conditions, had been studied[18], which was vital for high-temperature applications. The results showed that the oxidation resistance of $Hf_xTa_{1-x}C$ solid solutions was better than that of the constituent carbides. In addition, in our recent work, the oxidation behavior of a class of quinary TMC solid-solution ceramics was investigated and they exhibited a good and parabolic oxidation behavior[19, 20]. Nevertheless, there are few reports on the oxidation behavior of ternary or quaternary TMC solid-solution ceramics up to now.

(Zr, Nb, Ti)C (ZNTC) solid-solution ceramics, as a class of ternary TMC solid-solution ceramics, are expected to be potential candidates for applications in thermal protection structures and engine parts in next-generation re-entry space vehicles due to their potential high hardness, good corrosion resistance, and high melting temperature[11]. Inspired by the low-temperature oxidation behavior of individual components in air[21, 22], the oxidation behavior of ZNTC was investigated at 1073~1473 K in air for the first time. The oxidation kinetics, phase composition, and microstructure evolution of ZNTC samples were investigated, as well as the oxidation mechanisms.

2 Experimental method

2.1 Preparation of ZNTC solid-solution ceramics

The commercially available ZrC, NbC, and TiC powders (99.9% purity, average particle size <3 μm, Shanghai Chao-Wei Nanotechnology Co., Ltd.) were utilized as raw materials for fabricating ZNTC solid-solution ceramics. The above three powders were mixed at an equimolar composition of ZrC : NbC : TiC = 1 : 1 : 1. More details of preparing ZNTC solid-solution ceramics were reported elsewhere[11].

2.2 Oxidation tests

Isothermal oxidation tests of the cubic ZNTC samples (3 mm×3 mm×3 mm) were performed at 1073~1473 K in air within a muffle furnace. After the furnace was heated up to the desired temperature, the ZNTC samples were put into the furnace for 20 min. Afterwards, the samples were taken out at the designated time and cooled at room temperature in air to measure their weights. This cyclic oxidation tests were repeated for six times in total to ensure the oxidation time at each temperature reached 120 min. An electronic balance with a sensitivity of ±0.1 mg was used to examine and record the weight changes of ZNTC samples. The oxidation behavior of ZNTC samples was determined using the calculated weight gain per unit area as a function of time. In that case, whether the oxidation behavior of ZNTC samples followed a linear rate law or a parabolic rate law was determined by the following two equations:

$$(\Delta W/A) = k_l t \quad (1)$$

$$(\Delta W/A)^2 = k_p t \quad (2)$$

where ΔW is the weight change of ZNTC samples (mg), A is the area of ZNTC samples (cm^2), t is the holding time (min), and k_l and k_p are the linear and parabolic oxidation rate constants, respectively.

2.3 Characterization

The crystalline structure and morphology of ZNTC samples were analyzed by X-ray diffraction (XRD, X'pert PRO; PANalytical, Almelo, Netherlands) and scanning electron microscopy (SEM, supra-55; Zeiss, Oberkochen, Germany) with energy dispersive spectroscopy (EDS).

3 Results and discussion

Fig. 1a shows the specific weight change of ZNTC samples as a function of oxidation time at 1073~1473 K. It can be seen that the isothermal oxidation of ZNTC samples at 1073~1473 K is a weight gain process. Fig. 1b displays the plots of the square of the specific weight change of ZNTC samples as a function of oxidation time at different temperatures, from which a good linear relationship between the square of the specific weight change and oxidation time can be clearly seen. This suggests that the oxidation behavior of ZNTC samples at 1073~1473 K follows a parabolic rate law. That is to say, the oxidation of ZNTC samples is controlled by a diffusion process that the oxygen diffuses into the oxide layer. In general, the larger k_p is, the larger oxidation rate will be. Therefore, the k_p are further calculated and listed in Table 1. It clearly demonstrates that, with the increase of oxidation temperatures, k_p first show a small decrease from 1073 to 1173 K, followed by a significant increase from 1173 to 1273 K, and finally exhibit a continuous decrease from 1273 to 1473 K.

Fig. 2 shows XRD patterns of ZNTC samples before and after isothermal oxidation tests for 120 min at 1073~1473 K. At 1073 and 1173 K, the oxidation products of ZNTC samples are the same, namely ZrO_2, Nb_2O_5, and TiO_2 phases, except for the different polymorphs of TiO_2, namely anatase TiO_2(α-TiO_2)

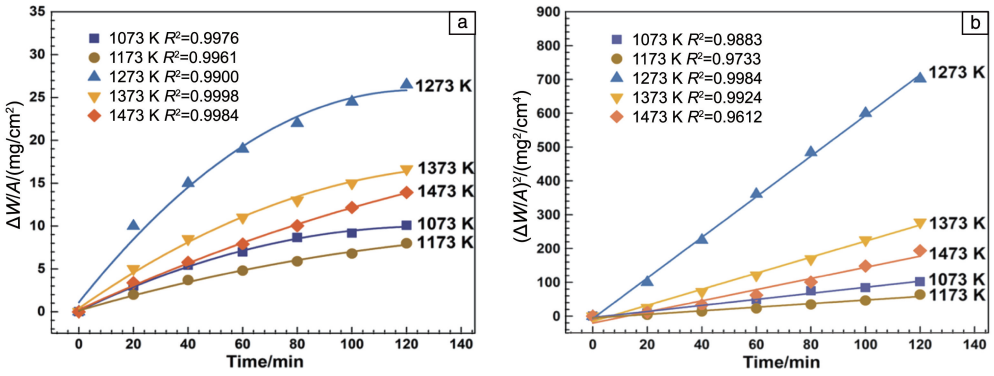

Fig. 1 Oxidation behavior of ZNTC samples at 1073 ~ 1473 K in air: (a) weight gain per unit surface area as a function of oxidation time, (b) the square of the specific weight change as a function of oxidation time

Table 1 The calculated parabolic rate constants (k_p) and the thickness of oxide layer of ZNTC samples

Oxidation temperatures/K	1073	1173	1273	1373	1473
k_p/($mg^2/cm^4 \cdot h$)	0.89	0.53	6.01	2.37	1.65
Oxide layer thickness/μm	272	114	520	435	180

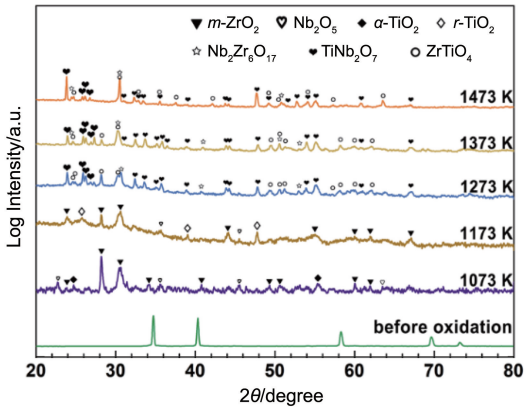

Fig. 2 XRD patterns of ZNTC samples before and after isothermal oxidation tests for 120 min at 1073 ~ 1473 K in air

and rutile TiO_2 (r-TiO_2). Therefore, the oxidation reaction of ZNTC samples at 1073 and 1173 K can be depicted by the following equation:

$$6(Zr_{1/3}Nb_{1/3}Ti_{1/3})C+\frac{19}{2}O_2 \longrightarrow 2ZrO_2+Nb_2O_5+2TiO_2+6CO \quad (3)$$

Nevertheless, when the oxidation temperatures are in the range of 1273 ~ 1473 K, the oxidation of ZNTC samples is varied and the corresponding oxidation products are mainly composed of the relatively complex $ZrTiO_4$, $TiNb_2O_7$, and $Nb_2Zr_6O_{17}$ phases, instead of the simple oxides observed at 1073 and 1173 K. As a result, the oxidation of ZNTC samples at 1273 ~ 1473 K can be described using the following reaction:

$$42(Zr_{1/3}Nb_{1/3}Ti_{1/3})C+\frac{133}{2}O_2 \longrightarrow 8ZrTiO_4+6TiNb_2O_7+Nb_2Zr_6O_{17}+42CO(g) \quad (4)$$

Typical SEM surface images of ZNTC samples after isothermal oxidation tests at 1073 ~ 1473 K for 120 min are shown in Fig. 3. Low-magnification SEM images (Fig. 3a, 3c, 3e, 3g, and 3i) show that, with an increasing of the oxidation temperatures from 1073 to 1473 K, the size and density of the microcracks on the formed oxide layers first exhibit an increase tendency from 1073 to 1273 K, and then gradually decrease with the further increase of the oxidation temperatures until no microcracks are observed at 1473 K. High-magnification SEM images (Fig. 3b and 3d) present that the formed oxide layers at 1073 and 1173 K possess a relatively dense microstructure, in which the grain shows a tendency to coarsen with the oxidation temperatures increasing from 1073 to 1173 K. This dense microstructure results in a decrease in the open porosity of the formed oxide layers from 1073 to 1173 K, which inhibits the diffusion of oxygen through the oxide layer. However, as the oxidation temperatures increase to 1273 K, the formed oxide layers possess a very high porosity, in which a large number of small pores are readily visible, as shown in Fig. 3f. Subsequently, with the oxidation temperatures increasing further from 1273 to 1473 K, the grain size of the formed oxide layers increases rapidly, while the pores become smaller at 1373 K and finally disappear completely at 1473 K, as displayed in Fig. 3h and 3j.

Fig. 4 shows SEM cross-section images of ZNTC samples after isothermal oxidation tests at 1073 ~ 1473 K. It is interesting to note that only the oxide layer formed at 1273 K exhibits a laminated structure while other formed oxide layers show a dense microstructure. Although the laminated structure is observed in the oxide layer formed at 1273 K, the formed oxide

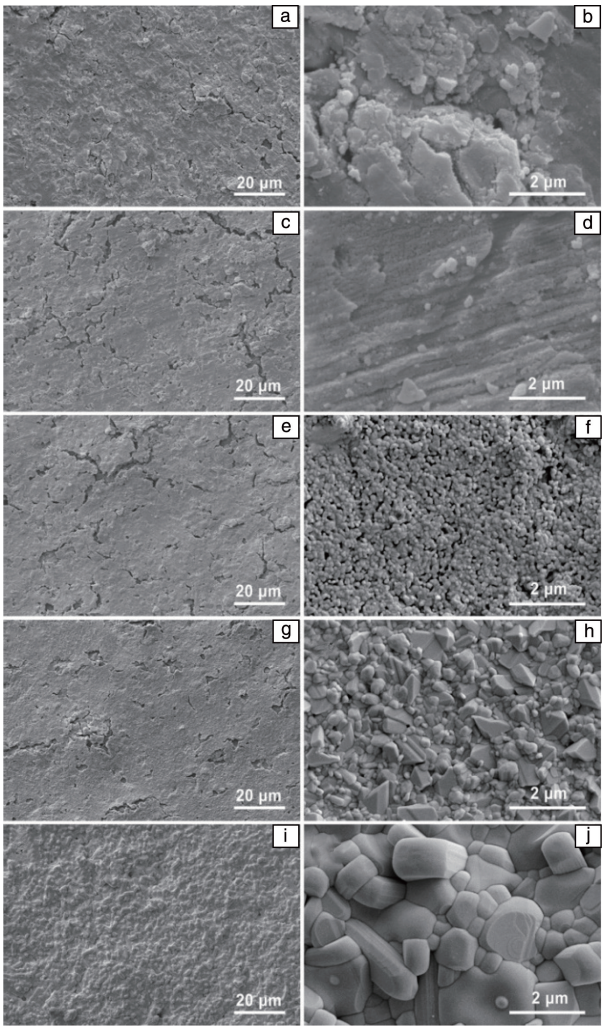

Fig. 3　SEM surface images of ZNTC samples after isothermal oxidation tests for 120 min at different temperatures: (a, b) 1073 K, (c, d) 1173 K, (e, f) 1273 K, (g, h) 1373 K, (i, j) 1473 K

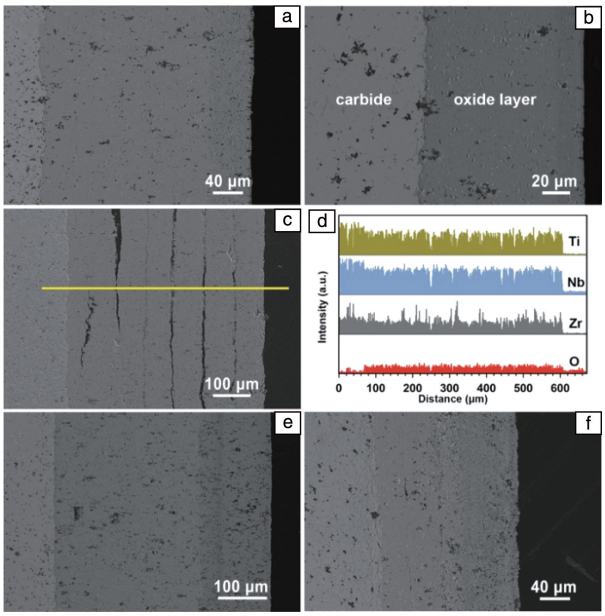

Fig. 4　SEM cross-section images of ZNTC samples after isothermal oxidation tests for 120 min at different temperatures: (a) 1073 K, (b) 1173 K, (c) 1273 K, (e) 1373 K, (f) 1473 K; element line scanning analysis of fig. 4c (yellow line) (d)

layer adheres closely to the substrate and no interfacial cracks can be found between them (Fig. 4c). Meanwhile, it is also worthy to note that no through-thickness cracks are observed in all formed oxide layers. In addition, as shown in Table 1, with the increase of the oxidation temperature, the thickness of the formed oxide layers first shows a decrease tendency from 1073 to 1173 K and then exhibits a sharp increase from 1173 to 1273 K, followed by a continuous decrease from 1273 to 1473 K. These observations are in good agreement with the variation in k_p at 1073 ~ 1473 K. The element line scanning analysis (Fig. 4d) shows that all the oxide layers consist of Zr, Nb, Ti, and O elements are distributed uniformly.

The evolution between laminated and dense structures in the formed oxide layers can be interpreted as follows: during the isothermal oxidation tests, an oxide layer is first generated on the substrate surface due to the oxidation of ZNTC substrate. Owing to the fact that the Pilling-Bedworth ratio of oxide layer to the substrate is in the range of 1 ~ 2[20], compressive stress from the oxide layer is generated on the pristine carbide. This is expected to improve the interfacial bonding between the oxide layer and the substrate and further restrain the generation of the interfacial cracks. As a result, no interfacial cracks are observed between the oxide layer and the substrate, as shown in Fig. 4. Nevertheless, owning to the mismatch of thermal expansion coefficients between the substrate and oxide layer, there are some residual thermal stresses in the formed oxide layer after the thermal cycling for weighing. In the next isothermal oxidation period, a new oxide layer is first generated between the substrate and the former oxide layer. In the following thermal cycling for weighing, whether the new oxide layer is delaminated from the former one is determined by the interaction between the residual thermal stress in the former oxide layer and the creep effect of the oxidation products. In general, the ratio of creep temperature to melting point of the inorganic materials is in the range of 0.4 ~ 0.5. On the basis of their melting points (Table 2), the creep temperatures of the oxidation products are calculated to be in the range of 919 ~ 1149 K below 1273 K and in the range of 848 ~ 1060 K above 1273 K, respectively. Obviously, when the oxidation temperatures are 1073 and 1173 K, which are comparative to or

slightly higher than the creep temperatures. Although the limited creep effect is produced, the generated residual thermal stress is also small in the former oxide layer due to the low oxidation temperatures. In that case, compared with the residual thermal stress, the impact of creep effect on the interfacial bonding between the new oxide layer and the former one is more significant. This can be responsible to the observations that no laminated oxide layer is observed at 1073 and 1173 K. When the oxidation temperatures increase to 1273 K, the creep effect is not enough to counteract the effect of the residual thermal stress, and this may lead to a delamination of the new oxide layer from the former one and finally causes the formation of the laminated oxide layer at 1273 K. By further elevating the oxidation temperatures up to 1373 and 1473 K, the oxidation temperatures largely exceed the creep temperatures of the oxidation products, and the creep effect dominates the interfacial bonding between the new oxide layer and the former one. As a consequence, the dense oxide layers without laminations are observed at 1373 and 1473 K.

According to XRD and SEM characterizations, it can be seen that the oxidation behavior of ZNTC samples at 1073 ~ 1473 K can be well interpreted by their phase composition and microstructure evolution. For the oxidized ZNTC samples, no interfacial cracks are observed between the substrate and oxide layer, as well as the through-thickness cracks in the oxide layer, as shown in Fig. 4. Above research further confirms that the oxidation process of ZNTC samples is controlled by a diffusion process that oxygen diffuses into the oxide layer. As a result, the oxidation process of ZNTC samples is mainly determined by the phase composition and microstructure evolution of the formed oxide layers. When the oxidation temperatures are below 1273 K, the oxidation products of ZNTC samples mainly include ZrO_2, Nb_2O_5, and TiO_2 phases. The formed oxide layer is relatively dense at 1073 K and thereby the corresponding oxidation rate is expected to be small (Table 1). As the oxidation temperatures increase to 1173 K, the grains of the oxide layer coarsen, which results in a decrease in the open porosity of the oxide layer and finally contributes to the decrease of the oxidation rate of ZNTC samples. When the oxidation temperatures are at or above 1273 K, the oxidation products of ZNTC samples primarily consist of the relatively complex $ZrTiO_4$, $TiNb_2O_7$, and $Nb_2Zr_6O_{17}$ phases. Interestingly, the oxide layer formed at 1273 K has a very high open porosity (Fig. 3f). For this reason, the oxidation rate of ZNTC sample is very large (Table 1). As the oxidation temperatures increase further from 1273 to 1473 K, the open porosity of the oxide layers is gradually and significantly reduced, owing to the rapid grain growth of oxidation products, which leads to the continuous and significant reduction in the oxidation rate of ZNTC samples, as displayed in Table 1. To sum up, the phase composition and microstructure evolution of the formed oxide layers is well expected to explain the observations in the temperature tendency of k_p.

Table 2 The melting points of oxidation products at 1073 ~ 1473 K[23-26]

Oxidation products	1073 ~ 1173 K			1273 ~ 1473 K		
	ZrO_2	Nb_2O_5	TiO_2	$ZrTiO_4$	$TiNb_2O_7$	$Nb_2Zr_6O_{17}$
Melting points/K	2988	1764	2143	2113	2155	2093

4 Conclusion

In conclusion, the isothermal oxidation behavior of ZNTC samples has been investigated at 1073 ~ 1473 K in air for 120 min. The oxidation of ZNTC samples shows a weight gain process with a parabolic rate law at 1073 ~ 1473 K in air. It is worth noticing that the calculated parabolic rate of ZNTC samples first exhibits a slow decrease tendency with the oxidation temperatures increasing from 1073 to 1173 K, followed by a rapid increase at 1273 K, and afterwards shows a gradual decrease with the oxidation temperatures increasing from 1273 to 1473 K. This tendency is expected to be resulted from the phase composition and microstructure evolution of the formed oxide layers. In addition, all the oxide layers exhibited the dense microstructure along the thickness direction without laminations except for at 1273 K. This could be explained by the interplay between the residual thermal stress in the generated oxide layers and the creep effect of the oxidation products during the isothermal oxidation tests.

参考文献 References

[1] FAHRENHOLTZ W G, HILMAS G E. Scripta Materialia[J], 2017,

129: 94-99.

[2] LIU J, HANG X, ZHANG G J, *et al*. Journal of the American Ceramic Society[J], 2013, 96(6): 1751-1756.

[3] KIM J, KIM M, ROH K, *et al*. Journal of the American Ceramic Society[J], 2019, 102(10): 6298-6308.

[4] FENG L, FAHRENHOLTZ W G, HILMAS G E, *et al*. Journal of the American Ceramic Society[J], 2019, 102(10): 5786-6795.

[5] SMITH C J, YU X X, GUO Q, *et al*. Acta Materialia[J], 2018, 145: 142-153.

[6] ZHANG C, GUPTA A, SEAL S, *et al*. Journal of the American Ceramic Society[J], 2017, 100(5): 1853-1862.

[7] WEINBERGER C R, THOMPSON G B. Journal of the American Ceramic Society[J], 2018, 101(10): 4401-4424.

[8] JIANG J, WANG S, LI W. Journal of the American Ceramic Society [J], 2016, 99(10): 3198-3201.

[9] ZHANG B, YIN J, CHEN J, *et al*. Journal of European Ceramic Society[J], 2018, 38: 1227-1236.

[10] REZAEI F, KAKROUDI M G, SHAHEDIFAR V, *et al*. Ceramic International[J], 2017, 43(17): 15537-15543.

[11] YE B, CHU Y, HUANG K, *et al*. Journal of the American Ceramic Society[J], 2019, 102(3): 919-923.

[12] DEMIRSKYI D, BORODIANSKA H, SUZUKI T S, *et al*. Scripta Materialia[J], 2019, 164: 12-16.

[13] CASTLE E, CSANÁDI T, GRASSO S, *et al*. Scientific Reports[J], 2018, 8(1): 8609-8612.

[14] YE B, WEN T, HUANG K, *et al*. Journal of the American Ceramic Society[J], 2019, 102(7): 4344-4352.

[15] YE B, WEN T, NGUYEN M C, *et al*. Acta Materialia[J], 2019, 170: 15-23.

[16] HARRINGTON T J, GILD J, SARKER P, *et al*. Acta Materialia[J], 2019, 166: 271-280.

[17] NING S, WEN T, YE B, *et al*. Journal of the American Ceramic Society[J], 2020, 103(3): 2244-2251.

[18] ZHANG C, BOESL B, AGARWAL A. Ceramic Internation[J], 2017, 43(17): 14798-14806.

[19] YE B, WEN T, CHU Y. Journal of the American Ceramic Society[J], 2019, 153(7): 327-332.

[20] YE B, WEN T, LIU D, *et al*. Corrosion Science[J], 2019, 153: 327-332.

[21] GASPARRINI C, CHATER R, HORLAIT D, *et al*. Journal of the American Ceramic Society[J], 2018, 101(6): 2638-2652.

[22] AHIMADA S, KOZEKI M. Journal of Materials Science[J], 1992, 27: 1869-1875.

[23] LI M, XU Q, WANG L. Ceramic International[J], 2012, 38(5): 4357-4361.

[24] SAMARANCH B, PISCINA P R, CLET G, *et al*. Chemistry of Materials[J], 2007, 19(6): 1445-1451.

[25] MARFUNIN A S. Physics of Minerals and Inorganic Materials[M]. Berlin: Springer, 1979.

[26] MESTRES L, MARTÍNEZ-SARRIÓN M L, CASTANO O, *et al*. Zeitschrift für Anorganische und Allgemeine Chemie[J], 2001, 627: 294-298.

(编辑 费蒙飞)